JOURNAL OF APPLIED ELECTROCHEMISTRY 14 (1984) 379–387

Electrochemical behaviour of the surface treated composite-electrolyte/electrode interface

S. P. S. BADWAL

CSIRO, Division of Materials Science, Advanced Materials Laboratory, PO Box 4331, Melbourne, Victoria, Australia 3001

Received 30 August 1983

The effect of surface treatment of the solid electrolyte 50 wt % (4.7 mol % Sc_2O_3 + 95.3 mol % ZrO_2) + 50 wt % Al_2O_3 (used in the $SIRO_2$ low temperature oxygen sensor) on its electrochemical behaviour has been studied by complex impedance spectroscopy. Two techniques, namely, preferential etching of alumina from the surface by a suitable etchant and cosintering of a thin layer of an alumina free electrolyte composition were used. The electrode/electrolyte interfaces prepared by using surface treated electrolyte samples had much lower electrode resistance (by a factor of 3–6) compared with the untreated surfaces. The decrease in the interfacial impedance is attributed mainly to the absence of alumina at the interface (an insulator phase) at which no oxygen exchange reactions could take place.

1. Introduction

Oxygen sensors based on stabilized zirconia electrolytes are in common use to measure, monitor and control oxygen in numerous industrial and laboratory environments. The sensor consists of an O^{2-} conducting solid electrolyte and two electrodes reversible to O_2/O^{2-} redox equilibria. If both electrodes of such a cell are exposed to different oxygen partial pressures, an e.m.f. develops which with respect to air as a reference atmosphere is given by the Nernst equation:

$$E(\text{mV}) = 0.049\,6T\log(0.21/p_{O_2}) \qquad (1)$$

where p_{O_2} is the unknown oxygen partial pressure. The need to attain thermodynamic equilibrium with respect to ambient atmosphere at both electrodes and at the same temperature requires the use of long impervious electrolyte tubes and the ducting of the reference gas to the sensing location. The zirconia tubes have low resistance to thermal and mechanical shocks and are expensive.

As a cheaper alternative, hermetic seals are formed between an electrolyte disc (or thimble) and a more robust ceramic (e.g. alumina) or metal (such as Kovar) tube of the required length and diameter by a metal–ceramic bonding technique [1, 2]. These seals are fragile and frequently fail in hostile industrial environments, e.g. noble metal seals in reducing atmospheres and reactive metal seals in oxidizing conditions.

Another commonly used technique is to fuse a solid electrolyte disc onto one end of a quartz tube [3]. The joints formed in such a way are often not leak-tight, have a short life and are suitable mainly for metallurgical applications.

A new technique developed in this laboratory involves joining a solid electrolyte pellet or disc to an alumina tube of the required length and diameter by a high temperature eutectic welding operation [4, 5]. The sensors thus prepared are rugged in construction, have low leak rates and are suitable for most industrial and laboratory applications. Unlike zirconia tubes, these sensors are far less susceptible to thermal and mechanical shocks.

A 4.7 mol % Sc_2O_3 + 95.3 mol % ZrO_2 composition containing 50 wt % Al_2O_3 is used as the solid electrolyte in the low temperature form of our sensor. The electrolyte also contains 4–15 wt % monoclinic zirconia (m-ZrO_2). The addition of alumina is necessary to increase the mechanical strength and, along with the m-ZrO_2, to reduce the thermal expansion mismatch between the electrolyte and the alumina tube sufficiently to allow a stable weld to form. This

0021-891X/84 $03.00 + .12

composition was selected on the basis of thermal expansion, leak rate and acoustic emission experiments [6]. The selection was made at the expense of a considerable drop in the electrolyte conductivity. Moreover, about 60% of the apparent electrode/electrolyte contact area is covered by alumina where virtually no oxygen exchange reactions can take place. Thus the presence of alumina, in addition to reducing the electrolyte conductivity, has a detrimental effect on the electrode kinetics as shown by the observed high interfacial impedance of sensors prepared with this composition. This high electrode impedance together with the already high electrolyte resistance make the sensors prone to noise pick-up at low temperatures, especially in an industrial environment. However, if the concentration of the insulator alumina phase at the electrode/electrolyte interface can be decreased, a considerable reduction in the electrode resistance is possible.

In this paper two techniques of producing an alumina-free electrolyte surface have been investigated. These are:

i. preferential etching of alumina by orthophosphoric acid and

ii. cosintering of a thin layer of alumina-free scandia-zirconia on the electrolyte surface.

The electrochemical behaviour (electrode and electrolyte) of the electrolyte samples has been studied by complex impedance spectroscopy.

2. Experimental procedures

The base electrolyte discs of 50 wt % (4.7 mol % Sc_2O_3 + 95.3 mol % ZrO_2) + 50 wt % Al_2O_3 (4.7 ScZ Al) were prepared by isostatically pressing the physically mixed oxide powders in a 12.5 mm steel die at a pressure of 200 M Nm^{-2}. For cosintering experiments some of these discs were coated on both sides with a paste of 7.75 mol % Sc_2O_3 + 92.25 mol % ZrO_2 (7.75 ScZ) in ethanol. The 7.75 ScZ paste was prepared by heating the coprecipitated hydroxides of scandium and zirconium at 1700° C for 12 h and then grinding the reacted powder in ethanol. Both virgin and coated discs were sintered at 1700° C (15 h). The discs for etching experiments were ground flat, polished (1 μm diamond powder) and etched with orthophosphoric acid at 350° C for five minutes [7]. These discs were cleaned with distilled water and heated again at 1700° C (15 h). The reason for this second heat treatment will become clear in the later sections.

The electrodes used were either porous Pt(sputter coated, ~ 0.9 μm thick) or a mixture (PtU2) comprising 75 wt % $(U_{0.38}Sc_{0.62})O_{2\pm x}$ + 25 wt % PtO_2 [8, 9]. The latter was in the form of a fine paste in ethylene glycol and was applied to the electrolyte discs with a paint brush. The coated discs were sandwiched between two annular Pt foil contacts for complex impedance measurements. The details of cell preparation are given in Table 1. At the start of an experiment the cell was slowly heated to 700° C and allowed

Table 1. Details of cell preparation

Cell	*Electrode*	*Surface preparation*	*Electrolyte dimensions* a/l *($cm^2 cm^{-1}$)*	*Coating*
1	sputtered Pt	Polished (1 μm diamond powder)	0.74/0.13	none
2	sputtered Pt	Etched	0.75/0.13	none
3	sputtered Pt	Etched heat-treated	0.74/0.13	none
4	sputtered Pt	Etched heat-treated	0.73/0.13	none
5	sputtered Pt	as fired	0.77/0.16	none
6	sputtered Pt	as fired	0.75/0.16	7.75 ScZ
7	sputtered Pt	as fired	0.75/0.17	7.75 ScZ
8	PtU2	20 μm (silicon carbide paper)	0.40/0.46	none
9[a]	PtU2	20 μm (silicon carbide paper)	0.34/0.51	none
10	PtU2	as fired	0.73/0.15	none
11	PtU2	as fired	0.43/0.18	7.75 ScZ

[a] Electrolyte sample was given an additional heat treatment at 1800° C for 20 min.

Table 2. Results of m-ZrO_2 measurements on electrolyte discs

Cell	m-ZrO_2 (%)	
	Side 1	*Side 2*
1	14	–
2	17	–
3	57	44
4	46	48

to equilibriate for 40–60 h in an atmosphere of pure oxygen. Complex impedance spectra were recorded several times during this period to study the effect of time on the electrode resistance. After it had stabilized (40–60 h), the data were recorded during cooling between 700 and 500° C at 25–50° C intervals. Two to three hours were allowed after each temperature change for thermal equilibrium conditions to re-establish. A Solartron frequency response analyser 1174 was ued in the fully-automated mode over the frequency range 1×10^{-3}–1×10^{6} Hz for complex impedance measurements [10]. The voltage applied across the cell was less than 10 mV r.m.s.

The electrolyte surfaces were characterized by carrying out *X*-ray analysis with a Rigaku diffractometer, using Cu $K\alpha$ radiation, and by examining the surfaces with a Hitachi S-450 LB scanning electron microscope.

The m-ZrO_2 content at the electrolyte surfaces was determined by comparing the areas under the monoclinic 1 1 1 and 1 1 $\bar{1}$ peaks with that under the tetragonal 1 1 1 peak* (Table 2) [11].

3. Characterization

3.1. *Etched samples*

Scanning electron micrographs of the etched electrolyte surfaces showed the presence of large rectangular crystals uncharacteristic of zirconia (Figs. 1a, b). Energy dispersive analysis by *X*-rays indicated that the etched surfaces were virtually free of Al_2O_3 [7]. *X*-ray diffractograms of these surfaces, however, revealed the presence of a significant proportion of another phase. The peak positions and relative intensities of this new phase

* Based on nonstandard face centred cubic cell.

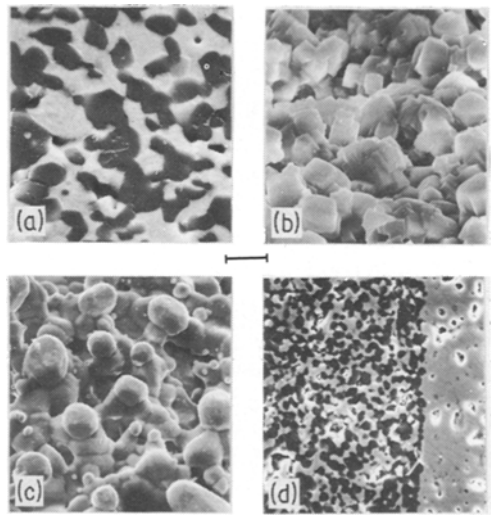

Fig. 1. Scanning electron micrographs of (a) polished (b) freshly etched, (c) etched heat-treated (1700° C, 15 h) electrolyte surfaces and (d) cross section of a cosintered sample. The dark areas in a and d represent alumina phase. Bar = 5 μm for a, b and c; and bar = 15 μm for d.

agreed with those of ZrP_2O_7. During etching with phosphoric acid, the reaction at the surface of the electrolyte was not confined to the alumina phase alone, a significant amount of zirconia was also attacked.

ZrP_2O_7 exists in three forms [12, 13], all of cubic symmetry. Form I is stable below 250° C but transforms irreversibly to Form II above 250° C. Alternatively, Form II can be directly obtained by heating ZrO_2 with orthophosphoric acid at $T > 250$° C. Form III exists only above 300° C and the Form II → Form III transformation is reversible. Diffraction patterns of Forms I and II are identical except for the presence of additional weak super lattice lines in the case of Form II [13]. From the diffractometer trace it was almost impossible to distinguish between Forms I and II. However, for our etching conditions Form II is most likely to be present on the electrolyte surface at room temperature. Form II has a tripled cubic unit cell (compared with Forms I and III) with cell parameter (a_0) of 24.735 Å [13]. The large unit cell results from the ordering of P_2O_7 anions. According to Harrison *et al.* [14], ZrP_2O_7 loses P_2O_5 when heated at 1550° C and is converted to $(ZrO)_2P_2O_7$. The latter phase is stable to at least 1600° C.

In the present study heat treatment of the etched samples at 1700° C (15 h) resulted in the complete disappearance of ZrP_2O_7 lines in the room temperature *X*-ray diffraction pattern and a corresponding increase in the intensity of the m-ZrO_2 lines. The intensities of the reflections from the tetragonal Sc_2O_3–ZrO_2 phase [15], however, remained virtually unchanged. Measurements of m-ZrO_2 content at the surfaces of these etched and heat-treated samples showed a much higher concentration of m-ZrO_2 (Table 2). Scanning electron micrographs of the heat-treated samples also showed quite clearly the rounding off of the rectangular ZrP_2O_7 crystals (Fig. 1c). These observations clearly suggest that, due to the high temperature treatment, the ZrP_2O_7 phase had decomposed to m-ZrO_2. Complex impedance measurements were made on two such samples which had been heated to 1700° C after etching and on one freshly etched sample with sputtered Pt electrodes.

3.2. *Cosintered samples*

The cosintered samples had an adherent, mechanically strong and uniform layer of the painted powder on the base electrolyte discs after sintering. The scanning electron micrograph in Fig. 1d shows the cross-section of a cosintered sample. *X*-ray diffraction patterns of the surfaces of the cosintered samples showed almost complete disappearance of Al_2O_3 and m-ZrO_2 lines. These results clearly indicated that the electrolyte surface was free of the insulator alumina phase and that the entire electrode/electrolyte contact area was now available for oxygen exchange reactions.

4. Results and discussion

4.1. *Effect of time on the cell impedance*

For all samples the electrode resistance increased with time during the inital 40–50 h after the cell had been heated to 700° C. This type of behaviour is commonly observed for noble metal electrodes and results from sintering and grain growth of the noble metal particles, leading to a reduction in the 2-phase electrode–electrolyte and 3-phase gas–electrode–electrolyte contact areas. The electrolyte resistance also increased during this time, but less significantly. The increase in the electrolyte resistance can also be assigned to the reduction in 2-phase and 3-phase contact areas which would add a small constriction resistance to the overall electrolyte resistance [16, 17].

4.2. *General behaviour*

For all cells the electrode arc was neither a perfect semicircle nor was it symmetrically distributed in the complex plane. In fact, the electrode arc was somewhat distorted on the high frequency side of the impedance spectrum. The data analysis to determine the total electrode resistance of a distorted arc has been described previously [18]. The difference between the right and the left intercepts of the electrode arc on the real axis ($R_1 - R_2 = R_0$) represents the total electrode resistance (Fig. 2).

4.3. *Electrode behaviour of etched samples*

Fig. 3 shows the response of sputtered Pt electrodes in contact with polished (a) and freshly etched (b) 4.7 ScZ–Al electrolyte discs in the complex impedance plane at 700° C. The electrode resistance of the latter cell (Cell 2) was orders of magnitude higher than that of the former (Cell 1). As discussed previously, the etchant used in the present study (orthophosphoric acid) preferentially removed alumina from the electrolyte surface and also attacked the Sc_2O_3–ZrO_2 phase, resulting in the formation of a large amount of ZrP_2O_7. The ZrP_2O_7 appears to have limited oxygen exchange capabilities with the electrode and acted as a barrier layer to the flow of charge across the interface. Upon decomposition of ZrP_2O_7 to m-ZrO_2, due to high temperature treatment at

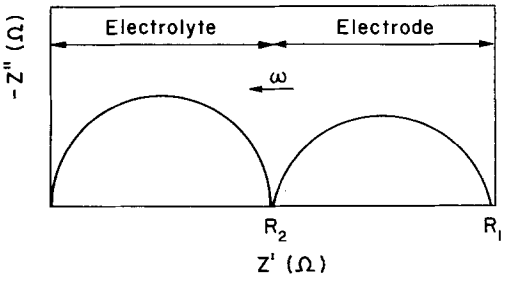

Fig. 2. The overall complex impedance behaviour.

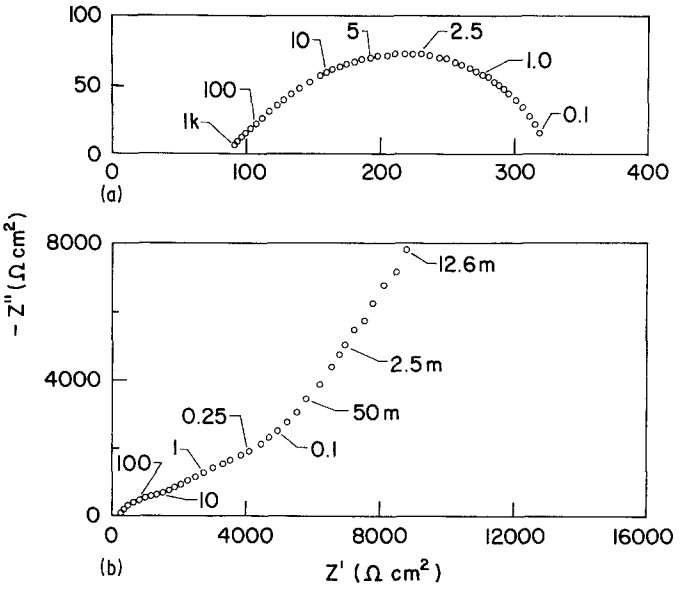

Fig. 3. Complex impedance spectra of (a) Cell 1 and (b) Cell 2 at 700° C in pure oxygen. The numbers on the arcs are frequencies in Hz.

1700° C, the electrode resistance decreased markedly as shown by the impedance spectra in Fig. 4 and Arrhenius plots of the electrode resistance (R_0) in Fig. 5. In fact the electrode resistance of the etched heat-treated samples was much lower than that of the polished unetched samples despite the presence of a significant amount of m-ZrO_2 at the interface in the case of the former.

Scanning electron micrographs of the electrode–electrolyte surfaces of Cells 1, 3 and 4 taken after complex impedance measurements are shown in Fig. 6 and reveal quite clearly that the electrode–electrolyte surface texture of Cell 3 (Figs. 6c, d) and Cell 4 (Figs. 6e, f) was considerably rougher than that of Cell 1 (Figs. 6a, b). Thus the decrease in the electrode resistance of etched heat-treated samples can be attributed to both the surface roughness effects and the absence of insulator alumina phase at the electrolyte surface. Both these effects would result in an increase in the useful area for oxygen exchange reactions at the electrode/electrolyte interface.

The observed differences in the electrode resistance of Cells 3 and 4 are probably due to the different texture of the electrolyte surface produced during etching which in turn gave different electrode microstructures. The electrode microstructure for Cell 4 was certainly more porous with extensive 3 phase gas–electrode–electrolyte contact boundary (Figs. 6e, f) compared with that for Cell 3 (Figs. 6c, d) and may have been the main cause for the low electrode resistance of this cell. Both the electrolyte samples were prepared, heat-treated (before and after etching) and sputtered with Pt electrodes under exactly identical conditions. However, minor variations in the etching conditions may have

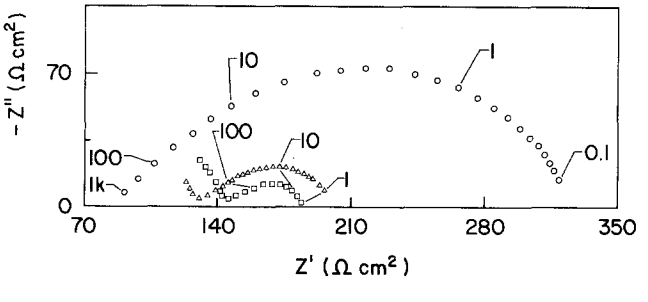

Fig. 4. Complex impedance spectra of ○ Cell 1, △ Cell 3, □ Cell 4 at 700° C in pure oxygen. The numbers on the arcs are frequencies in Hz.

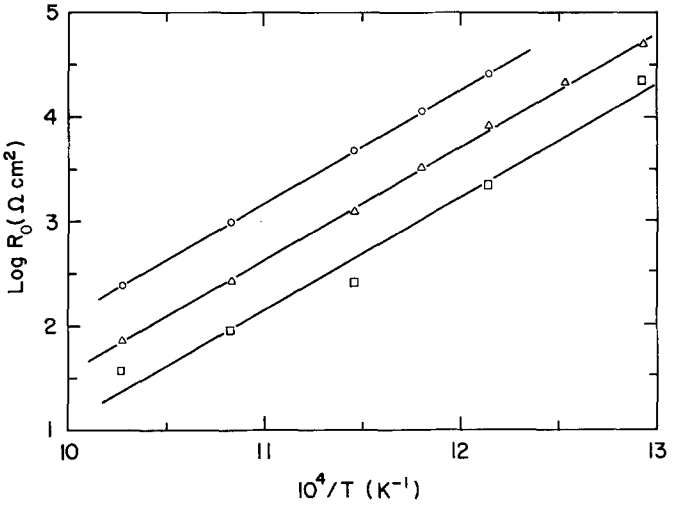

Fig. 5. Arrhenius plots for the electrode resistance of ○ Cell 1, △ Cell 3, □ Cell 4.

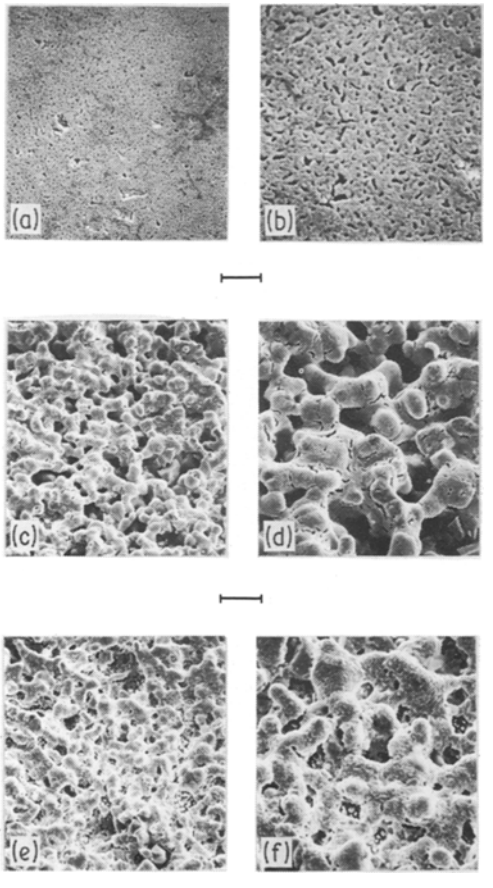

Fig. 6. Scanning electron micrographs of polished (a and b) and etched-heat treated (Cell 3 – c and d, Cell 4 – e and f) electrode–electrolyte surfaces after complex impedance measurements. For a, c and e bar = 15 μm, for b, d and f bar = 6.0 μm).

produced different electrolyte surfaces. This view is supported by the observed difference in the m-ZrO_2 content on the opposite faces of the electrolyte sample used in Cell 3 (Table 2). Since most of the m-ZrO_2 in the etched heat-treated samples is formed by the decomposition of ZrP_2O_7, it is reasonable to assume that both surfaces of the electrolyte sample used in Cell 3 were attacked differently by phosphoric acid, thus producing different amounts of ZrP_2O_7.

Despite enormous differences in the electrode–electrolyte contact area, surface texture, etc., for Cells 1, 3 and 4, the activation energies (Table 3) for the electrode resistance were quite similar, indicating that the same process was responsible for the oxygen exchange reaction at the electrode/electrolyte interface.

4.4. *Electrode behaviour of cosintered samples*

The electrode responses for Cells 5–7 (Pt electrodes) in the complex impedance plane at 650° C in pure oxygen are shown in Fig. 7 and Arrhenius plots for the electrode resistance are given in

Table 3. Activation energy for total electrode resistance

Cell	E *(kJ mol^{-1})*
Cell 1	208 ± 2
Cell 3	208 ± 3
Cell 4	202 ± 18

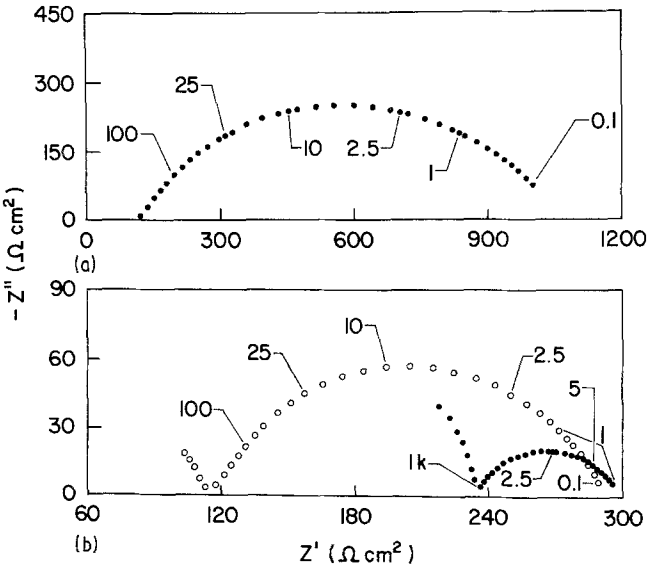

Fig. 7. Complex impedance plane plots for the electrode behaviour at 650° C in pure oxygen of (a) • Cell 5 and (b) ○ Cell 6 and • Cell 7. The numbers on the arcs are frequencies in Hz.

Fig. 8. The electrode/electrolyte interfacial resistance of Cells 6 and 7 which used electrolytes prepared by cosintering a layer of 7.75 ScZ on 4.7 ScZ–Al was significantly lower than that of Cell 5. The electrode behaviour of sputtered Pt electrodes on microscopically rough electrolyte surfaces, however, was complicated and, over the temperature range of the present study, it appears that two processes with different activation energies contribute to the electrode reaction.

Cells with PtU2 electrodes showed a much lower interfacial resistance than those with sputtered Pt electrodes irrespective of whether the electrolyte surface was virgin or cosintered. Cell 11 with a cosintered layer of 7.75 ScZ and PtU2 electrodes had a much lower electrode resistance than Cells 8, 9 and 10 with similar electrodes but no cosintered layer on the electrolyte (Fig. 9). These results clearly demonstrate that considerable improvements to the interfacial properties of $SIRO_2$ oxygen sensors can be achieved.

4.5. *Electrolyte behaviour*

For etched samples the presence of ZrP_2O_7 in Cell 2 and that of m-ZrO_2 in Cells 3 and 4 at the electrolyte surface resulted in higher electrolyte resistance (left intercept of the electrode arc on

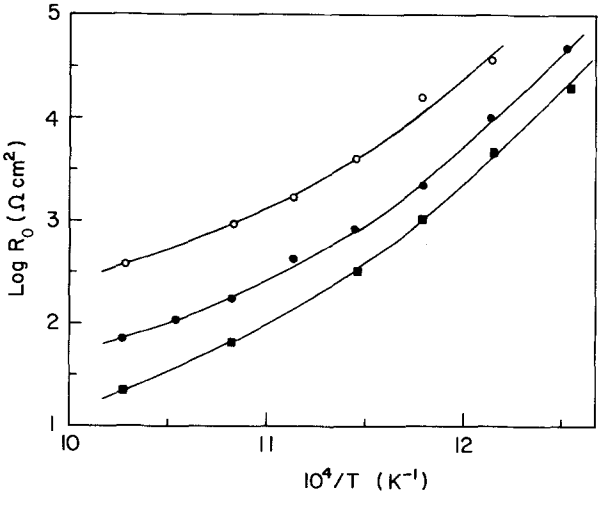

Fig. 8. Arrhenius plots for the electrode resistance (sputtered Pt electrodes) of ○ Cell 5, • Cell 6 and ■ Cell 7.

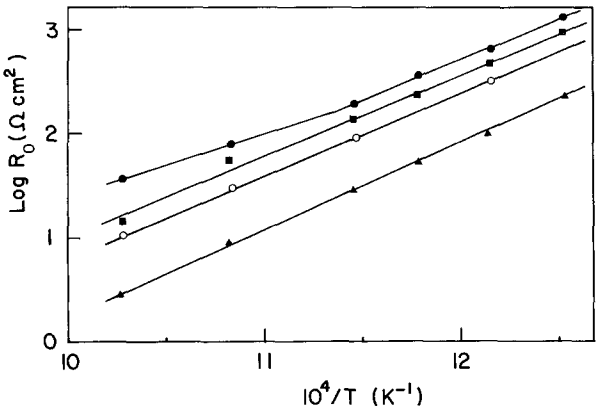

Fig. 9. Arrhenius plots for the electrode resistance (PtU2 electrodes) of • Cell 8, ▪ Cell 9, ○ Cell 10 and ▲ Cell 11.

the real axis, R_2), compared with the values observed for the unetched electrolyte (Cell 1) (Fig. 4). The presence of the m-ZrO_2 phase is undesirable as it masks a part of the reduction in the electrode resistance achieved by etching.

The total electrolyte resistance of cosintered samples, however, was lower by a factor of ~ 2 compared with that for the uncoated electrolyte discs (Fig. 10). Preliminary analysis of the overlapping electrolyte arcs (grain boundary and lattice conductivity) indicates that it is the grain boundary arc which was mainly affected. Complex impedance and microstructural work is in progress to understand this intriguing behaviour.

5. Conclusions

Reduction in the concentration of Al_2O_3 at the electrode/electrolyte interface by both etching and cosintering techniques results in a dramatic decrease in the electrode resistance. With the etching technique a part of the decrease in the electrode resistance is masked by the increase in the electrolyte resistance due to the presence of the poorly-conducting m-ZrO_2 phase at the surface. This problem may be solved by the incorporation of a thin layer of Sc_2O_3 or Sc_2O_3-rich ZrO_2 phase at the surface after etching but prior to decomposition of the ZrP_2O_7. This, however, will make the etching technique laborious and expensive. Moreover, a fine control of the etching conditions is absolutely necessary. The cosintering technique on the other hand is less time consuming, cheap and can be easily adapted to the mass production of oxygen sensors.

Perhaps the significance of this work can be more easily realized in the field of fuel cells and steam electrolysers where current carrying capacities of these devices as well as the mechanical strength and thermal shock resistance of the electrolyte are very important. The latter two properties can be achieved either by the addition of 10–20 wt % Al_2O_3 to fully stabilized zirconia or the use of partially stabilized zirconia (PSZ), although at the expense of considerable reduction in the electrolyte conductivity in the latter case. Nevertheless the incorporation of a material with better oxygen exchange capabilities

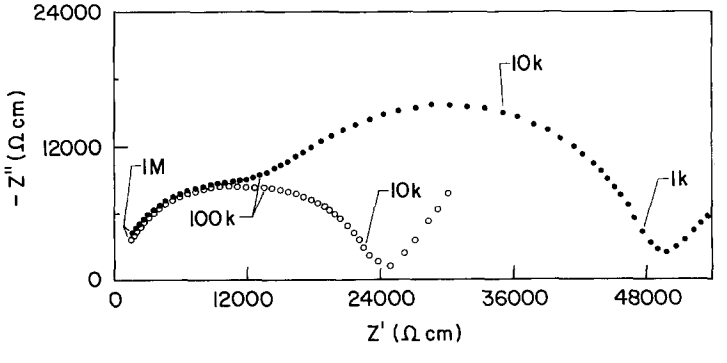

Fig. 10. The electrolyte behaviour at 450° C of • uncoated and ○ cosintered sample in pure oxygen. The numbers on the arcs are frequencies in Hz.

at the surface of the aforementioned electrolytes should reduce the interfacial impedance, with a corresponding decrease in the overpotential losses and an increase in the efficiency of fuel cells and stream electrolysers.

Acknowledgement

The author is thankful to Mr W. G. Garrett and Dr J. Drennan for critical review of this manuscript and Mr R. C. Wotherspoon for etching the electrolyte samples. Partial support for this project was provided under the National Energy Research Development and Demonstration Program which is administered by the Commonwealth Department of National Development and Energy of Australia.

References

[1] H. J. de Bruin, A. F. Moodie and C. E. Warble, *J. Mater. Sci.* 7 (1972) 909.
[2] F. P. Bailey and W. E. Borbidge, 'Materials Science Research,' Vol. 14 (edited by J. Park and A. Evans) Plenum Press, New York (1980) p. 525.
[3] B. Deo and V. B. Tare, *J. Sci. Ind. Res.* **30** (1971) 465.
[4] R. K. Stringer and K. A. Johnston, US Patent No. 4 046 661 (1977).
[5] M. J. Bannister, N. A. McKinnon and R. R. Hughan, US Patent No. 4 193 857 (1980).
[6] W. G. Garrett, Proceedings of the Tenth Australian Ceramic Society Conference, Melbourne, Australia, 24–27 August, 1982, p. 339.
[7] R. C. Wotherspoon, CSIRO, Division of Materials Science, Report No. AML-83-56.
[8] S. P. S. Badwal and M. J. Bannister, Australian provisional patent application No. 7857/83.
[9] S. P. S. Badwal, M. J. Bannister and W. G. Garrett, Proceedings of Zirconia Technologies Conference, Stuttgart, 21–23 June, 1983.
[10] S. P. S. Badwal, CSIRO Division of Materials Science, Report No. AML-83-49.
[11] R. C. Garvie and P. S. Nicholson, *J. Amer. Ceram. Soc.* **55** (1972) 303.
[12] C. Huang, O. Knop, D. A. Othen, F. W. D. Woodhams and R. A. Howie, *Can J. Chem.* **53** (1975) 79.
[13] M. Chaunac, *Bull. Soc. Chem. Fr.* (1971) 424.
[14] D. E. Harrison, H. A. McKinstry and F. A. Hummel, *J. Amer. Ceram. Soc.* **37** (1954) 277.
[15] M. J. Bannister and P. Skilton, *J. Mater. Sci. Letters* **2** (1983) 561.
[16] M. Kleitz, H. Bernard, E. Fernandez and E. Schouler, 'Advances in Ceramics', Vol. 3 (edited by A. H. Heuer and L. W. Hobbs) The American Ceramic Soc. Inc., Columbus, Ohio, (1981) p. 310.
[17] H. Tannenberger and H. Siegert, *Adv. Chem. Series* **90** (1969) 281.
[18] S. P. S. Badwal, *J. Electroanal. Chem.* in press.